



**HAL**  
open science

## On the potential of $^{230}\text{Th}$ , $^{231}\text{Pa}$ , and $^{10}\text{Be}$ for marine rain ratio determinations: A modeling study

C. Heinze, M. Gehlen, C. Land

### ► To cite this version:

C. Heinze, M. Gehlen, C. Land. On the potential of  $^{230}\text{Th}$ ,  $^{231}\text{Pa}$ , and  $^{10}\text{Be}$  for marine rain ratio determinations: A modeling study. *Global Biogeochemical Cycles*, 2006, 20 (2), pp.n/a-n/a. 10.1029/2005GB002595 . hal-03113025

**HAL Id: hal-03113025**

**<https://hal.science/hal-03113025>**

Submitted on 18 Jan 2021

**HAL** is a multi-disciplinary open access archive for the deposit and dissemination of scientific research documents, whether they are published or not. The documents may come from teaching and research institutions in France or abroad, or from public or private research centers.

L'archive ouverte pluridisciplinaire **HAL**, est destinée au dépôt et à la diffusion de documents scientifiques de niveau recherche, publiés ou non, émanant des établissements d'enseignement et de recherche français ou étrangers, des laboratoires publics ou privés.

## On the potential of $^{230}\text{Th}$ , $^{231}\text{Pa}$ , and $^{10}\text{Be}$ for marine rain ratio determinations: A modeling study

C. Heinze,<sup>1</sup> M. Gehlen,<sup>2</sup> and C. Land<sup>3,4</sup>

Received 26 July 2005; revised 1 February 2006; accepted 8 March 2006; published 16 June 2006.

[1] The global distributions of the radionuclides  $^{230}\text{Th}$ ,  $^{231}\text{Pa}$ , and  $^{10}\text{Be}$  are simulated with a biogeochemical ocean general circulation model. Sensitivity experiments for changes in the composition of the particle composition ratio (POC:CaCO<sub>3</sub>:BSi:clay, POC = particulate organic carbon, CaCO<sub>3</sub> = calcium carbonate, BSi = biogenic silica) are carried out with and without biogeochemical feedback. The absolute water column concentrations of the radionuclides react significantly to changes in the particle rain composition. The radionuclide ratio in the sediment, however, is less sensitive to changes in the particle composition ratio. Still, selected areas could record composition ratio changes reliably for paleo reconstructions. Measurements of  $^{230}\text{Th}$ ,  $^{231}\text{Pa}$ , and  $^{10}\text{Be}$  in the water column have the potential to monitor changes in the large scale CaCO<sub>3</sub> production which may occur as a consequence of ocean acidification due to oceanic uptake of anthropogenic CO<sub>2</sub>.

**Citation:** Heinze, C., M. Gehlen, and C. Land (2006), On the potential of  $^{230}\text{Th}$ ,  $^{231}\text{Pa}$ , and  $^{10}\text{Be}$  for marine rain ratio determinations: A modeling study, *Global Biogeochem. Cycles*, 20, GB2018, doi:10.1029/2005GB002595.

### 1. Introduction

[2] Despite major research efforts, such as JGOFS [e.g., *Hanson et al.*, 2000], exact quantifications of the vertical marine particle flux are still difficult to achieve. Among other factors, the high spatial and temporal variability of biogenic particle production at the sea surface as well as the potential errors associated with direct sediment trap measurements contribute to respective uncertainties in the flux measurements [e.g., *Antia et al.*, 2001; *Scholten et al.*, 2001]. Next to absolute rates of particle rain, the ratio of the different particle species is an important variable in earth system science. The marine particle flux consists of biogenic particulate organic carbon (POC) and biogenic shell material (opal or BSi = biogenic silica, CaCO<sub>3</sub> = calcium carbonate) and terrigenous material from river loads and dust deposition from the atmosphere (referred to here as “clay”). The ratio of elements in the particulate material which is exported vertically out of the euphotic zone, the composition ratio, POC:CaCO<sub>3</sub>:BSi:clay, varies in the ocean [e.g., *Dymond and Lyle*, 1985]. While in upwelling regions with high supply of silicic acid silica shell producing organisms (in particular diatoms) dominate export production, in oligotrophic regions, organisms which build calcareous shells dominate [e.g., *Baumann et al.*, 2005]. Further, the production of

CaCO<sub>3</sub> shell material is favored at higher temperatures and is less pronounced in colder regions.

[3] The variation in particle composition ratios is an important factor in the Earth system. A part of the glacial/interglacial pCO<sub>2</sub> signal in the atmosphere may be attributed to changes in the ratio of POC:CaCO<sub>3</sub>, though these composition ratio changes may probably not be the only cause of this signal [*Berger and Keir*, 1984]. Owing to the anthropogenic CO<sub>2</sub> emissions and the associated acidification of ocean waters, we potentially face the start of a significant reduction in pelagic CaCO<sub>3</sub> production [*Riebesell et al.*, 2000; *Heinze*, 2004]. It is a challenge to detect respective changes in the POC:CaCO<sub>3</sub>:BSi flux in the ocean.

[4] Marine distributions of reactive metals are a potentially useful tool for assessing changes in marine particle composition ratios [*Chase et al.*, 2002, 2003; *Luo and Ku*, 1999]. The long-living radioisotopes  $^{230}\text{Th}$ ,  $^{231}\text{Pa}$ , and  $^{10}\text{Be}$  (half-life  $7.5 \times 10^4$  yr,  $3.2 \times 10^4$  yr,  $1.5 \times 10^6$  yr, respectively) are of specific interest: Their source function is well defined ( $^{230}\text{Th}$ ,  $^{231}\text{Pa}$ ) or can be reconstructed sufficiently well ( $^{10}\text{Be}$ ), their particle reactivity is different (extreme, high, less high, respectively) and they are removed from the water column preferentially by different particle species which contribute to the vertical marine particle flux. The continuous source of the radionuclides is balanced by a continuous sink of these nuclides through loss to the sediment (plus a very small amount due to radioactive decay). The fraction of radionuclides which becomes attached to particles in the scavenging process, and the fraction which stays in solution within the water column depends on the particle composition and particle concentration (or reactive surface area available). For  $^{230}\text{Th}$  a preferential scavenging to CaCO<sub>3</sub> particle phases, while

<sup>1</sup>Geophysical Institute and Bjercknes Centre for Climate Research, University of Bergen, Bergen, Norway.

<sup>2</sup>Laboratoire des Sciences du Climat et de L'Environnement, UMR CEA-CNRS, Gif-sur-Yvette, France.

<sup>3</sup>Max Planck Institute for Meteorology, Hamburg, Germany.

<sup>4</sup>Now at Meteoterra GmbH, Rinteln/Exten, Germany.

for  $^{231}\text{Pa}$ , and  $^{10}\text{Be}$  preferential scavenging to opaline (siliceous) particle phases have been identified [Chase *et al.*, 2002, 2003]. Moreover Luo and Ku [1999] find a less pronounced scavenging of  $^{231}\text{Pa}$  to clay than for  $^{230}\text{Th}$ . The preferential scavenging cannot be regarded as strict. Recent studies with field data suggest that  $^{230}\text{Th}$ ,  $^{231}\text{Pa}$ , and  $^{10}\text{Be}$  are also attracted by organic matter [Li, 2005] and that preferential scavenging of  $^{230}\text{Th}$ ,  $^{231}\text{Pa}$  may vary regionally [Scholten *et al.*, 2005]. Also, for  $^{234}\text{Th}$  scavenging by colloidal organic matter was observed in the laboratory [Quigley *et al.*, 2002]. The same may apply for radionuclides in the real world, where for example diatoms are important producers of organic substances (such as transparent exopolymer particles TEP), and would complicate the inversion from radionuclide concentrations to particle species. In general, the smaller the particle reactivity is, the more the tracer concentration in the water column depends on the ocean circulation, as individual metal ions can travel for longer before being scavenged. At least three oceanic variables would be mapped on the radionuclide tracer distributions: the circulation, the biogenic particle export production, and the composition of the particles. We investigate here the potential of radionuclide distributions to reflect and record variations in the particle composition ratio. We focus in particular on variations in  $\text{CaCO}_3$  and BSi fluxes relative to those of POC and clay.

## 2. Model Description

[5] We employ here the Hamburg ocean carbon cycle circulation model HAMOCC [Maier-Reimer, 1993] in its computationally most economic form with an annual time step. This model is described in detail by Heinze and Maier-Reimer [1999] and Heinze *et al.* [1999] and further updates are given by Heinze *et al.* [2003]. The model has been previously successfully used for scavenging studies where a reproduction of the seasonal cycle is less important, but long integration periods are required [Gehlen *et al.*, 2003; Henderson *et al.*, 1999]. The model has a horizontal resolution of  $3.5^\circ \times 3.5^\circ$  and 11 layers (centered at 25, 75, 150, 250, 450, 700, 1000, 2000, 3000, 4000, and 5000 m). It includes representations of the marine carbon, oxygen, phosphorus, and silicon cycles. Prognostic variables in the water column are the concentrations of total dissolved inorganic carbon, alkalinity, dissolved phosphate, dissolved oxygen, dissolved organic carbon, particulate organic carbon, particulate inorganic carbon ( $\text{CaCO}_3$ ), biogenic silica, as well as the dissolved and particle attached phases of the three radionuclides  $^{230}\text{Th}$ ,  $^{231}\text{Pa}$ , and  $^{10}\text{B}$ . In the sediment we have the corresponding dissolved species as in the water column as prognostic variables in the pore water chemistry (except DOC) as well as the weight percentages of the solid sediment species organic carbon,  $\text{CaCO}_3$ , opal, and clay. All particle export production rates and particle fluxes are further predicted by the model. The global sediment accumulation rates in model equilibrium are fixed by input rates from the continents, while the local sediment accumulation rates are prognostic variables. A simple trophic model provides biogenic particle export production rates for POC,  $\text{CaCO}_3$ , and BSi. Marine clay flux is prescribed

according to aeolian dust deposition rates after Andersen *et al.* [1998]. The model water column is interactively coupled with an early diagenesis model simulating the bioturbated sediment zone and sediment accumulation. The velocity and thermohaline fields for driving the tracer transports were taken from the dynamical Large Scale Geostrophic model [Maier-Reimer *et al.*, 1993] in the preindustrial configuration of Winguth *et al.* [1999].

[6] Biogenic particle production is carried out as in Heinze *et al.* [1999], where both POC and BSi production follow Michaelis-Menten kinetics, but with separate uptake velocities. Phosphate is assumed to be the biolimiting nutrient for POC production. Through choice of a higher uptake velocity  $V_{\text{max}}^{\text{BSi}}$  of silicic acid for BSi production, than the phosphate uptake velocity for POC production differential patterns for new production of POC and BSi result with larger horizontal gradients for BSi export than for POC export [see also Heinze *et al.*, 1999],

$$P_{\text{POC}} = \frac{V_{\text{max}}^{\text{POC}} \cdot [\text{PO}_4^{3-}]^2 \cdot \text{Red}(C:P)}{K_s^{\text{POC}} + [\text{PO}_4^{3-}]} \quad (1)$$

$$P_{\text{BSi}} = \frac{V_{\text{max}}^{\text{BSi}} \cdot [\text{Si}(\text{OH})_4]^2}{K_s^{\text{BSi}} + [\text{Si}(\text{OH})_4]} \quad (2)$$

where

$P_{\text{POC}}$	POC export production, $\text{mol L}^{-1} \text{ yr}^{-1}$ ;
$\text{Red}(C:P)$	Redfield ratio C:P;
$V_{\text{max}}^{\text{POC}}$	maximum uptake rate of phosphate, $\text{yr}^{-1}$ ;
$K_s^{\text{POC}}$	half saturation constant for POC production, $\text{mol L}^{-1}$ ;
$P_{\text{BSi}}$	BSi export production, $\text{mol L}^{-1} \text{ yr}^{-1}$ ;
$V_{\text{max}}^{\text{BSi}}$	maximum uptake rate of silicic acid, $\text{yr}^{-1}$ ;
$K_s^{\text{BSi}}$	half saturation constant for BSi production, $\text{mol L}^{-1}$ .

[7] The export production of particulate inorganic carbon, i.e.  $\text{CaCO}_3$ , is then computed on the basis of the POC and BSi export production rates,

$$P_{\text{CaCO}_3} = P_{\text{POC}} \cdot r \cdot \left(1 - \frac{P_{\text{BSi}}/S}{P_{\text{POC}}}\right); \quad \frac{P_{\text{BSi}}}{P_{\text{POC}}} < S \quad (3)$$

with  $P_{\text{POC}}$ ,  $P_{\text{BSi}}$ , and  $P_{\text{CaCO}_3}$  the export production rates for POC, BSi, and  $\text{CaCO}_3$  and the tunable constants  $r$  as well as the threshold value  $S$ .  $r$  is the parameter which sets rain ratio  $C(\text{CaCO}_3):C(\text{organic C})$  in the absence of any dissolved silica. In cases that  $\frac{P_{\text{BSi}}}{P_{\text{POC}}}$  is larger than or equal to  $S$  the  $\text{CaCO}_3$  production is set to a minimum value of  $P_{\text{POC}} \cdot r \cdot 0.01$ . In the standard model version,  $r$  and  $S$  are set to 0.30 and 0.7, respectively.

[8] Scavenging of reactive metals is carried out according to the reversible first-order scavenging reaction [Gehlen *et al.*, 2003],

$$\frac{dc_{\text{part}}}{dt} = \kappa \cdot [c_{\text{part}}^{\text{EQ}} - c_{\text{part}}]$$

$$c_{\text{part}}^{\text{EQ}} = k_d \cdot c_{\text{diss}} \cdot P,$$

**Table 1.** Overview About Model Runs

Experiment Number	Acronym of Experiment	Description of Experiment	Parameter Change	CaCO <sub>3</sub> Export Production, GtC/yr	BSi Export Production, teramole Si/yr
1	R1	reference, no scavenging to POC	-	1.49	199
2	R2	reference, scavenging to POC	-	1.49	199
3	L1	low CaCO <sub>3</sub> :BSi, no scavenging to POC	$r/4$	0.37	205
4	L2	low CaCO <sub>3</sub> :BSi, scavenging to POC	$r/4$	0.37	205
5	H1	high CaCO <sub>3</sub> :BSi, no scavenging to POC	$V_{\max}^{BSi} \times *4$	1.78	148
6	H2	high CaCO <sub>3</sub> :BSi, scavenging to POC	$V_{\max}^{BSi} \times *4$	1.78	148

with  $c_{part}$  (in [mol/L]) the concentration of particle bound metal ( $^{230}\text{Th}$ ,  $^{231}\text{Pa}$ , and  $^{10}\text{Be}$ , respectively),  $c_{diss}$  (in [mol/L]) the concentration of dissolved metal,  $c_{part}^{EQ}$  (in [mol/L]) the equilibrium concentration of particle bound metal,  $\kappa$  (in [ $\text{yr}^{-1}$ ]) the first-order rate constant (here set to  $10^4 \text{ yr}^{-1}$  assuming a quasi-instantaneous reaction),  $k_d$  (in [L/kg]) the partitioning coefficient, and  $P$  (in [kg/L]) the concentration of suspended particulate material.

[9] We carried out two sets of standard or reference runs for two scenarios concerning particle species dependent scavenging. First, we made the simplifying assumption that  $^{230}\text{Th}$  is only scavenged by CaCO<sub>3</sub> and clay,  $^{231}\text{Pa}$  only by BSi, and  $^{10}\text{Be}$  only by BSi and clay. This simplification is appropriate, if one's goal is to see how large changes of radionuclide concentrations for given particle composition ratio changes could be in the ideal case. This reference run is called R1 (see Table 1). Second, we allowed that  $^{230}\text{Th}$ ,  $^{231}\text{Pa}$ , and  $^{10}\text{Be}$  are in addition to the previous species scavenged to POC. This reference run is called R2. For the partitioning coefficient  $k_d$  we follow the formulation of *Honeyman et al.* [1988],

$$\log_{10} k_d = a + b \cdot \log_{10} M,$$

where  $M$  is the particle concentration (here taken in  $\mu\text{g}$  particles per liter) and  $a$  as well as  $b$  are tunable parameters. We optimized the constants  $a$  and  $b$  for the partitioning coefficient independently for the two reference runs R1 and R2 with respect to observed data using the full three-dimensional model (Run R1:  $a_{Th-230} = 6.2741$ ,  $b_{Th-230} = 0.3919$ ;  $a_{Pa-231} = 5.4966$ ,  $b_{Pa-231} = 0.4192$ ;  $a_{Be-10} = 2.8419$ ,  $b_{Be-10} = 0.3614$ ; run R2:  $a_{Th-230} = 6.2713$ ,  $b_{Th-230} = 0.3916$ ;  $a_{Pa-231} = 5.4515$ ,  $b_{Pa-231} = 0.4208$ ;  $a_{Be-10} = 2.7963$ ,  $b_{Be-10} = 0.4001$ , for  $^{230}\text{Th}$ ,  $^{231}\text{Pa}$ , and  $^{10}\text{Be}$  respectively) (Figure 1). For  $^{230}\text{Th}$  and  $^{231}\text{Pa}$ , the same data set of observations as compiled from various authors for *Henderson et al.* [1999] was used, with the addition of Southern Ocean measurements from *Chase et al.* [2003]. For  $^{10}\text{Be}$ , measurements were taken from *Kusakabe et al.* [1987], *Ku et al.* [1990], and *Frank et al.* [2002], and *Chase et al.* [2003]. Under sea ice, also biogenic particle production was allowed, however using a reduction factor  $f_r$  for the nutrient uptake velocity in proportion to the sea ice thickness,

$$f_r = e^{(-d_{ice}/50)},$$

where  $d_{ice}$  is the sea ice thickness in cm. In the model, especially at high latitudes with small biological production rates, CaCO<sub>3</sub> production rates and hence also water column

CaCO<sub>3</sub> particle concentrations can approach zero or go to zero. We assumed that  $^{230}\text{Th}$  would also scavenge to BSi in case of a near depletion of CaCO<sub>3</sub> particles (CaCO<sub>3</sub> production under  $1 \mu\text{mol/L/yr}$ ), in order to avoid unrealistic high dissolved phase concentrations. As the results in or near ice covered regions appear to depend quite strongly on the choice of such a threshold value, and measurements that would justify the choice made would be highly desirable.

[10] As source functions, homogeneous constant production rates were applied for dissolved phases of  $^{230}\text{Th}$  and  $^{231}\text{Pa}$  ( $0.0468 \cdot 10^{-3}$  and  $1.89810^{-3}$  atoms  $\text{s}^{-1} \text{L}^{-1}$  respectively). Both  $^{230}\text{Th}$  and  $^{231}\text{Pa}$  result from the U decay series ( $\alpha$ -decay of dissolved  $^{234}\text{U}$  and  $^{235}\text{U}$ ). Owing to the long residence time of uranium in the ocean, it is almost perfectly mixed. The source function for  $^{10}\text{Be}$  differs fundamentally from those for  $^{230}\text{Th}$  and  $^{231}\text{Pa}$ :  $^{10}\text{Be}$  enters the ocean from the atmosphere at the surface and the flux of “new”  $^{10}\text{Be}$  into the ocean varies geographically with patterns of wet and dry deposition in a complex way.  $^{10}\text{Be}$  deposition rates for present-day were simulated with the

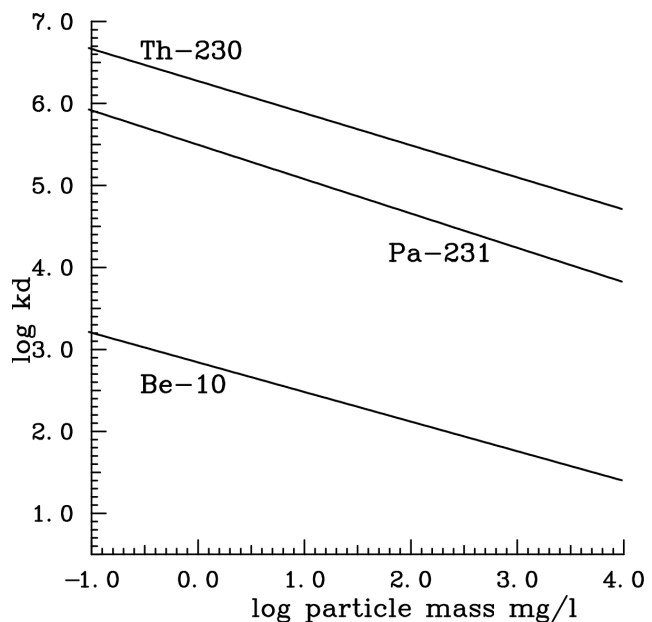


**Figure 1.** Equilibrium distribution coefficient  $k_d$  for the different radionuclides resulting from fit of the model (reference run R1) to observations. The values for reference run R2 are very similar to these values (see text).

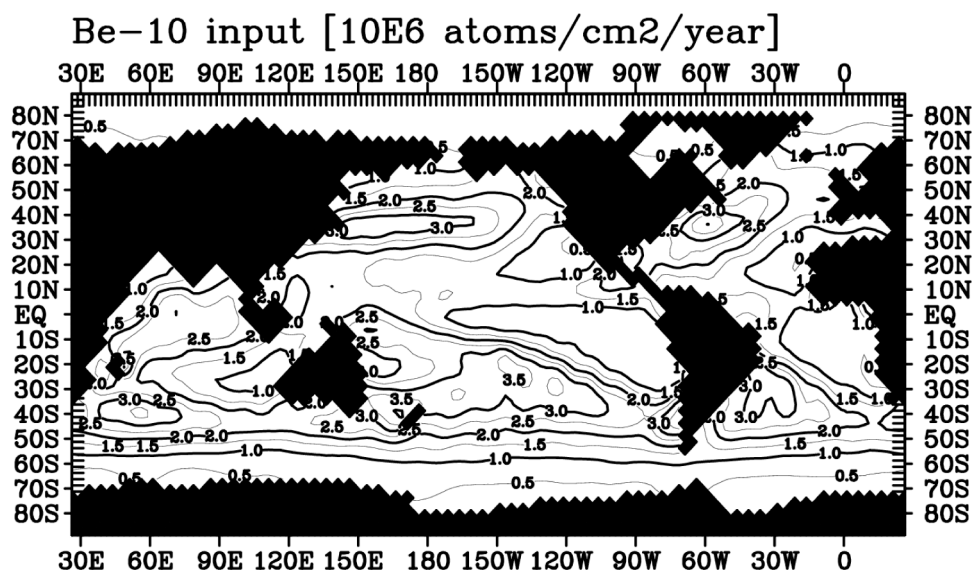


Figure 2. Annual mean deposition rate of  $^{10}\text{Be}$  onto the ocean surface as simulated by the MAECHAM4 model.

middle-atmosphere general circulation model MAECHAM4 [see *Land and Feichter*, 2003, and references therein]. The production rate of  $^{10}\text{Be}$  depends on the cosmic ray particle flux. Variations in the geomagnetic field intensity and the solar activity are therefore the dominant causes for time-dependent changes in the production rate. In the simulation of  $^{10}\text{Be}$  as used here, the production rate was prescribed according to *Masarik and Beer* [1999] for average solar years, and present geomagnetic field intensity. As the geomagnetic field acts as a shield, the production flux is highest around the magnetic poles and decreases towards lower latitudes. The production rate is zero at the top of the atmosphere. It increases towards the Earth's surface and reaches a maximum above the poles between about 10 and 20 hPa [*Masarik and Beer*, 1999]. As the cosmic ray flux is approximately anticorrelated to the solar activity, the production rate is underestimated (overestimated) in years with weak (strong) solar activity. *Masarik and Beer* [1999] and *Koch et al.* [1996] estimated a range in production variations due to solar variability of 15 to 25%. Using the  $^{10}\text{Be}$  production rates as prescribed by *Masarik and Beer* [1999] for average solar activity, the annual global production of  $^{10}\text{Be}$  in the ECHAM4 model simulation is 49.19 g/yr. This value is within the range of production rates given in the literature. *Lal and Peters* [1967] give a global production flux 120.2 g/yr for  $^{10}\text{Be}$  for years with low solar activity. *Oeschger et al.* [1969] determined a global  $^{10}\text{Be}$  production of 37.40 g/yr for average solar years. Very soon after their production,  $^{10}\text{Be}$  atoms attach to available aerosol particles. Transport into the troposphere and subsequent wet deposition is the main sink for  $^{10}\text{Be}$ . A smaller sink results from dry deposition. Wet and dry deposition are parameterized according to *Feichter et al.* [1991] and *Brost et al.* [1991]. For  $^{10}\text{Be}$  the percentage removal is 9% and 91% by dry and wet deposition, respectively. For our ocean model study the deposition flux from the

atmospheric circulation model were averaged annually (Figure 2).

### 3. Methodology

[11] The model was integrated in forward mode for 6 different cases. First of all, the two reference runs were provided: one without scavenging to POC and one with additional scavenging to POC (runs R1 and R2, Table 1). A previous model spin-up without radionuclide simulations was used as a basis. This run was integrated long enough so that water column and sediment are in quasi-equilibrium. Then the radionuclide module for  $^{230}\text{Th}$ ,  $^{231}\text{Pa}$ , and  $^{10}\text{Be}$  was added starting from zero concentrations for the dissolved as well as particle attached nuclide species. The model including radionuclides was then integrated for another 4000 years after the final adjustment for the scavenging constants. For R1 and R2 slightly different equilibrium partitioning coefficients were used as determined in the optimization with respect to observations.

[12] With respect to the reference runs (run R1 and R2), two sets of sensitivity experiments were carried out by varying the particle export production composition ratio. In the first set a lower export production ratio  $\text{CaCO}_3:\text{BSi}$  than in the reference runs was simulated (runs L1 and L2), in the second set a higher export production ratio  $\text{CaCO}_3:\text{BSi}$  (runs H1 and H2; see Table 1). Runs L1 and H1 were performed relative to reference run R1 (without scavenging to POC), runs L2 and H2 relative to run R2 (with additional scavenging to POC). In all runs, the radionuclides react to the change in the particle elemental ratios plus all internal adjustments of the oceanic biogeochemical system. In runs L1 and L2, the export production ratio  $\text{CaCO}_3:\text{BSi}$  (and thus also the ratio  $\text{CaCO}_3:\text{POC}$ ) was reduced by changing parameter  $r$  of equation (3) from 0.30 to a quarter of this value (Table 1). A respective export

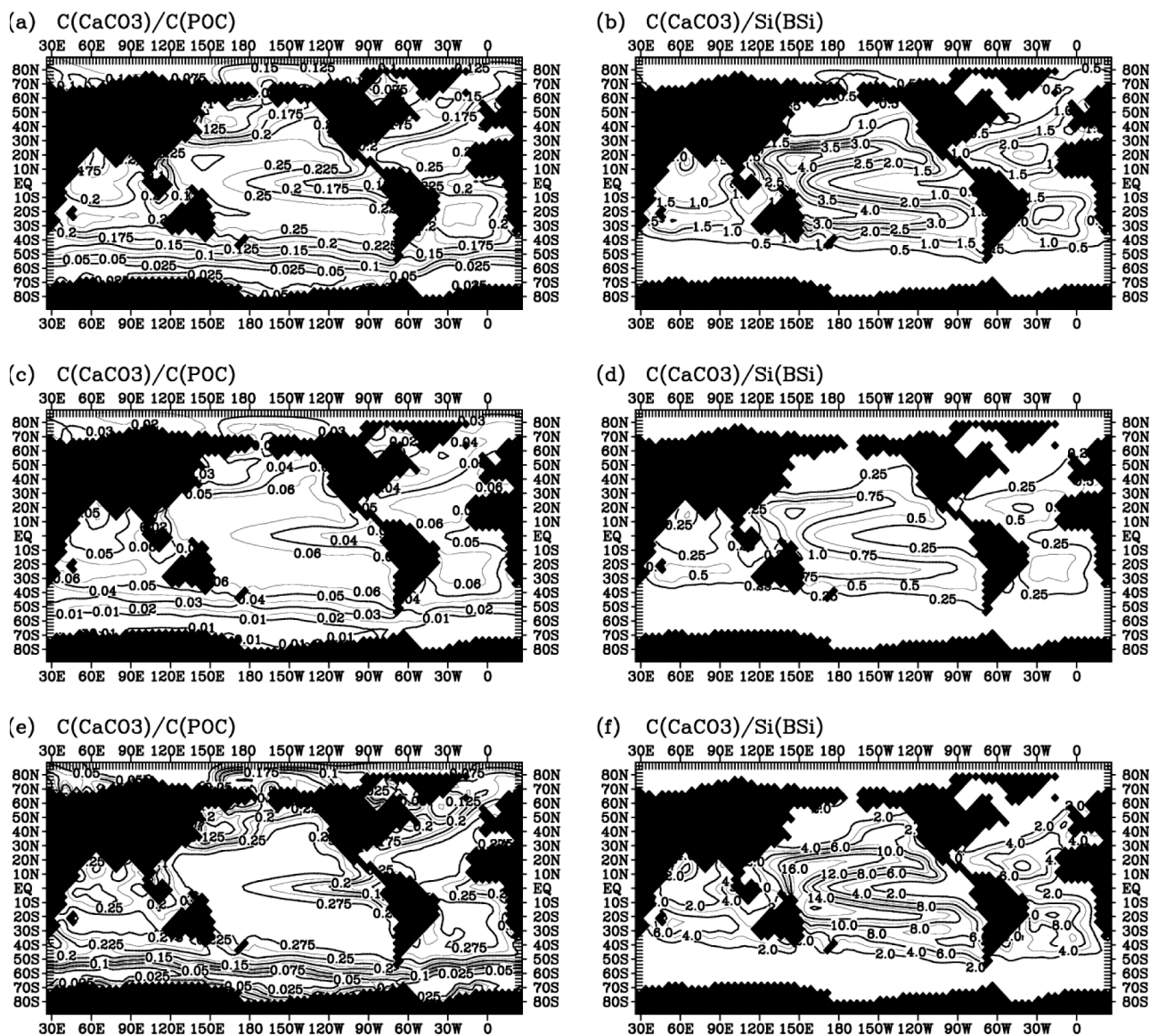


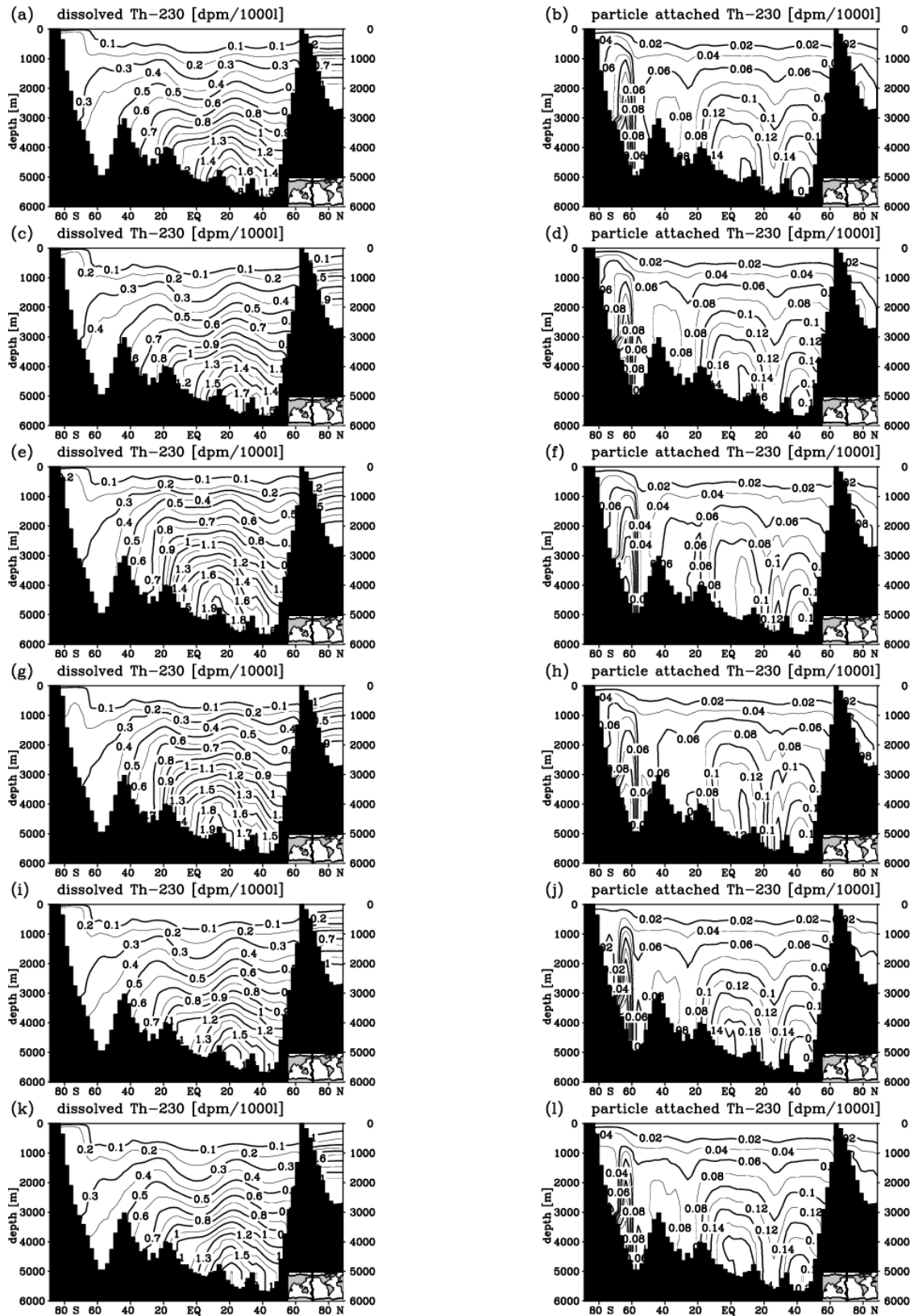
**Figure 3.** Export production composition ratios  $\text{CaCO}_3$ :POC and  $\text{CaCO}_3$ :BSi on a molar basis for (a, b) the reference run R1, (c, d) the run with reduced  $\text{CaCO}_3$ :BSi ratio L1, and (e, f) the run with increased  $\text{CaCO}_3$ :BSi ratio H1. The distributions for run R2, L2, and H2 are practically identical.

production ratio increase was simulated by quadrupling the uptake velocity of silicic acid for the production of BSi (runs H1 and H2, Table 1). This leads to considerably larger areas of the surface layer and subsurface ocean depleted with respect to silicic acid. The result is that at those locations the  $\text{CaCO}_3$ :BSi ratio increases both in the surface production as well as in the particle flux. All sensitivity experiments were restarted from the reference run and then integrated for 20,000 years in order to reequilibrate the biogeochemical state after the changes in the particle composition ratio parameterization (for the radionuclides themselves shorter integration times could be used, once the biogeochemical state of the ocean is in quasi-steady state again). The specification of the runs is summarized in Table 1. The rain ratios of  $\text{CaCO}_3$ :POC and the ratios  $\text{CaCO}_3$ :BSi as

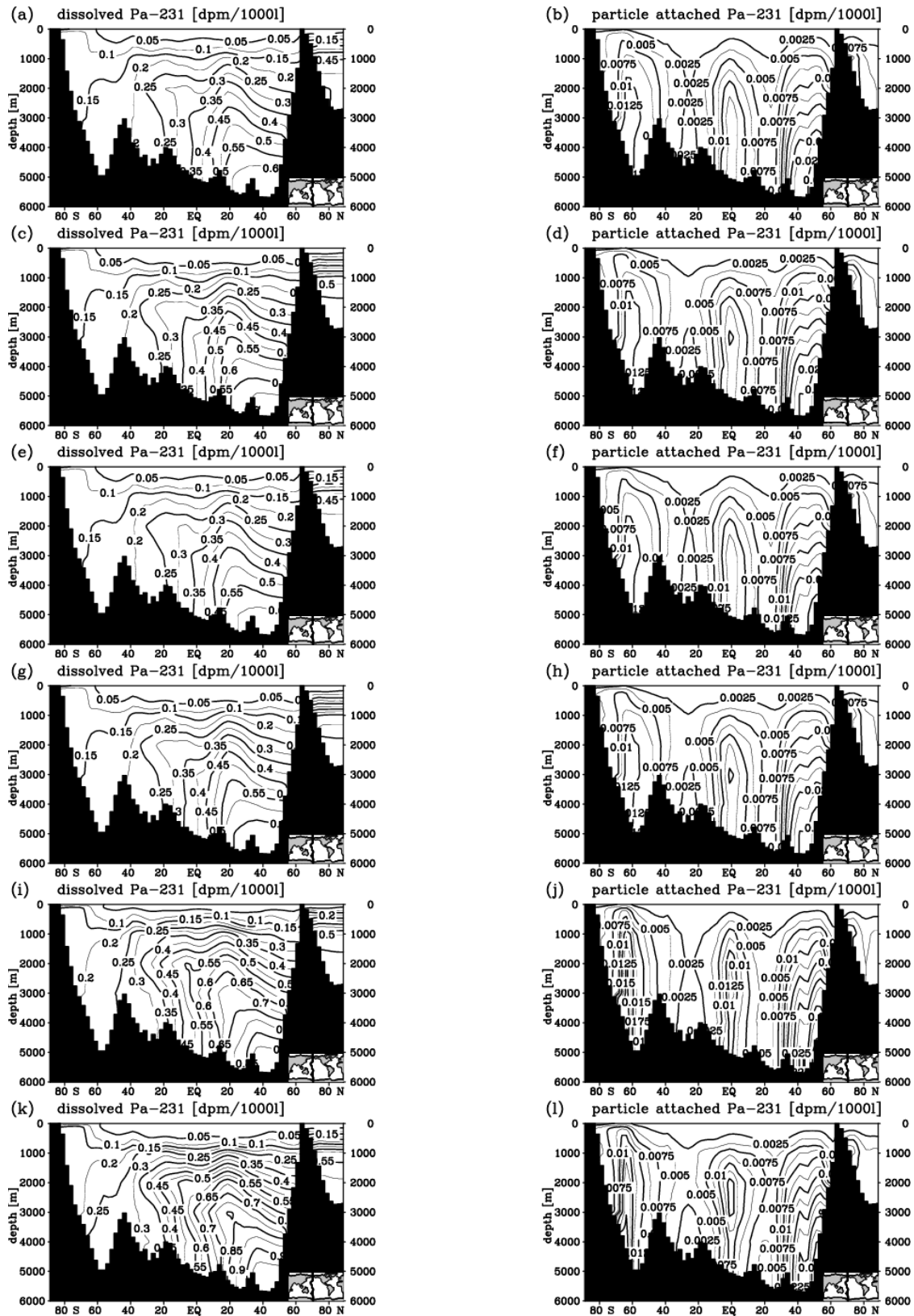
resulting for the reference run, and the sensitivity experiments with full feedback are given in Figure 3. Global production rates for  $\text{CaCO}_3$  and BSi are also listed in Table 1.

#### 4. Discussion of Results

[13] Three different radionuclide variables are of interest, if one aims at using variations for reconstructions of particle composition ratios: the water column concentrations of both the dissolved and particle attached phases, and the nuclide ratios in particulate matter that is deposited on the ocean floor and thus is entering the sediment. The first two variables are relevant for the modern ocean, while the nuclide ratios are the important variable for potential rain



**Figure 4.**  $^{230}\text{Th}$  concentrations in the (left) dissolved and (right) particle attached phases for the different model runs. (a, b) Run R1. (c, d) Run R2. (e, f) Run R1 minus L1. (g, h) Run R2 minus L2. (i, j) Run R1 minus H1. (k, l) Run R2 minus H2. See also Table 1 for specification of runs. Figures 4e–4l are difference plots.



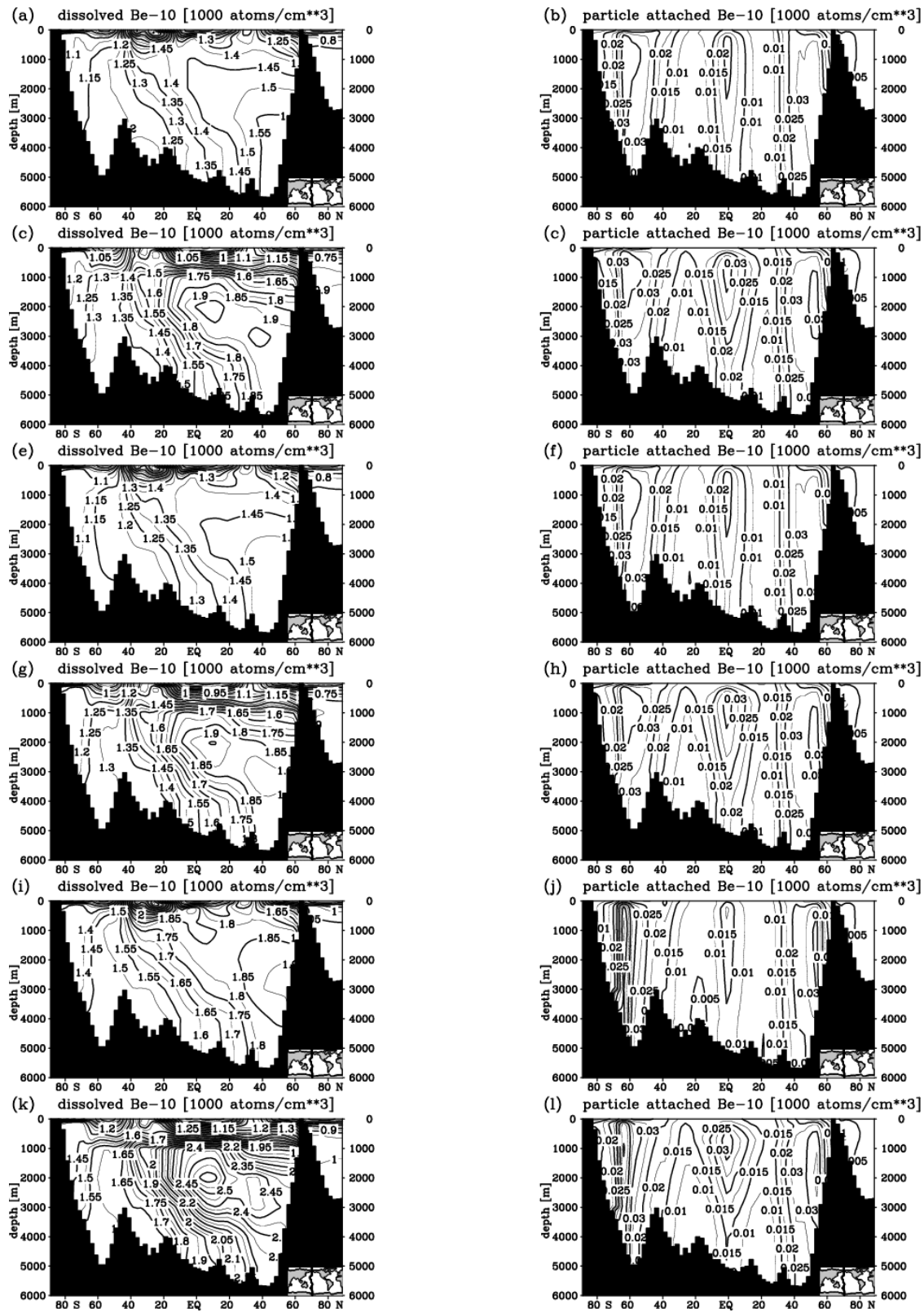


**Figure 6.**  $^{10}\text{Be}$  concentrations in the (left) dissolved and (right) particle attached phases for the different model runs. (a, b) Run R1. (c, d) Run R2. (e, f) Run R1 minus L1. (g, h) Run R2 minus L2. (i, j) Run R1 minus H1. (k, l) Run R2 minus H2. See also Table 1 for specification of runs. Figures 6e–6l are difference plots.

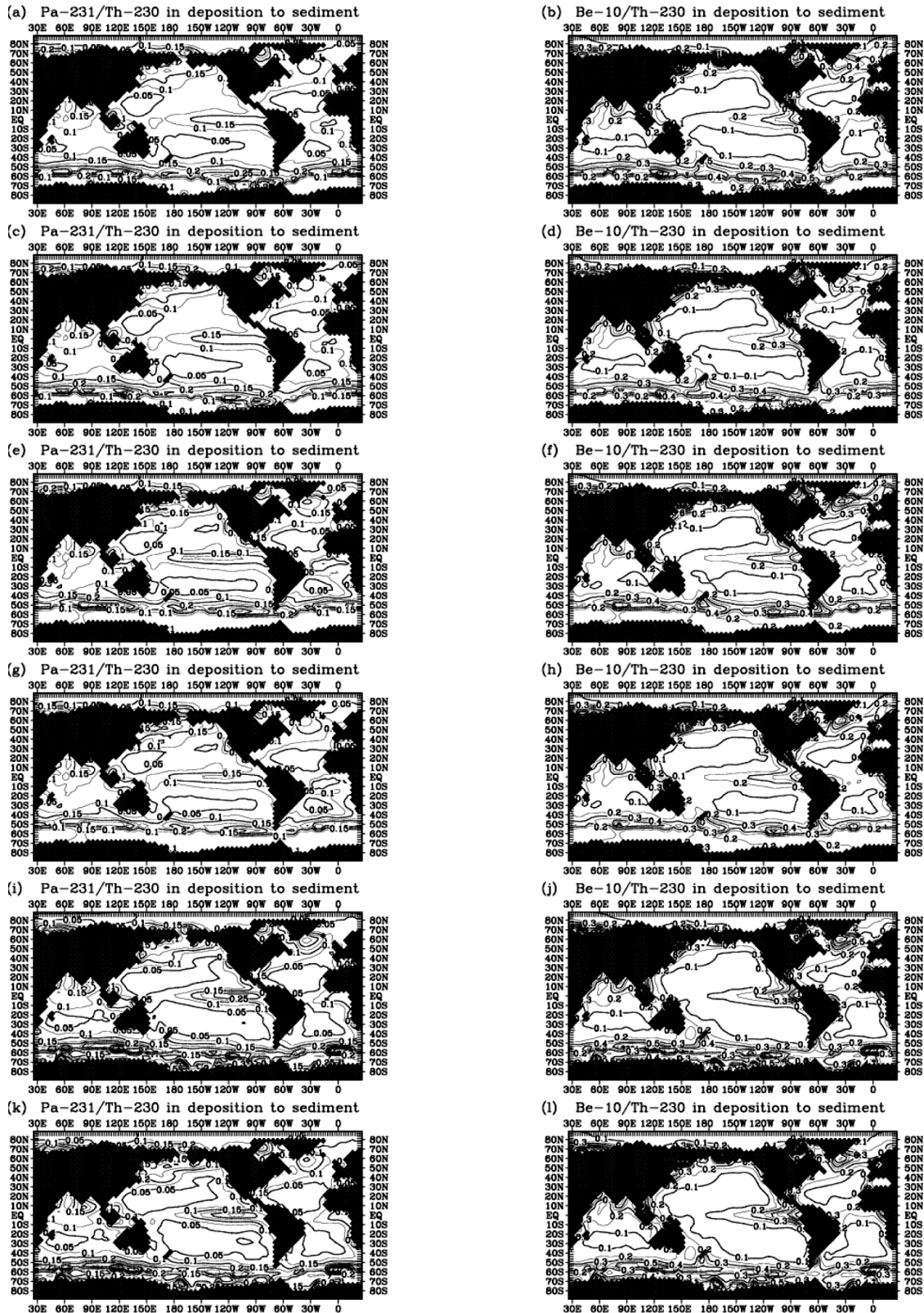
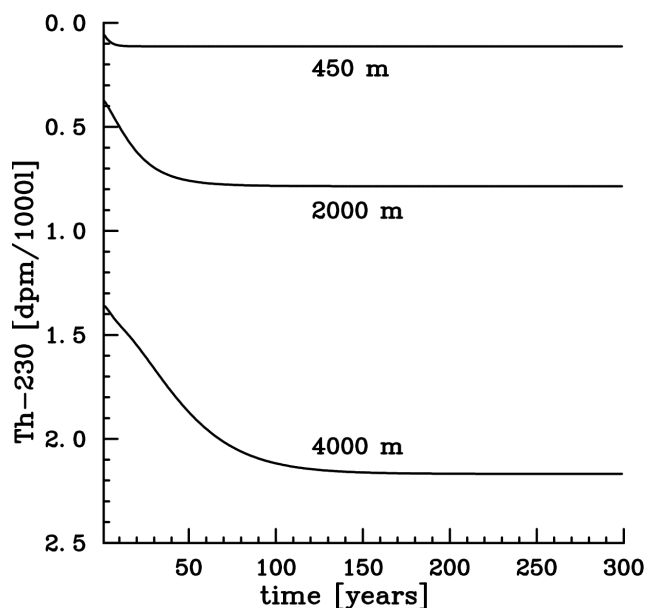


Figure 7. Nuclide ratios in sediment deposition: (left)  $^{231}\text{Pa}/^{230}\text{Th}$  and (right)  $^{10}\text{Be}/^{230}\text{Th}$ . (a, b) Run R1. (c, d) Run R2. (e, f) Run R1 minus L1. (g, h) Run R2 minus L2. (i, j) Run R1 minus H1. (k, l) Run R2 minus H2. See also Table 1 for specification of runs. Figures 7e–7l are difference plots.



**Figure 8.** Time series of  $^{230}\text{Th}$  (dissolved phase) for a grid point in the central Pacific Ocean ( $1.25^\circ\text{ N}$ ,  $148.75^\circ\text{ W}$ ). The time series starts at the perturbation of reference run R1 for experiment L1 with a strong reduction in the  $\text{CaCO}_3$  export production. The reaction is quickest in upper waters, while in deep waters the amplitude of the ratio is largest.

ratio reconstructions from the sediment core record. We have summarized meridional cross sections of the Pacific Ocean for the three radionuclides and the different sensitivity experiments in Figures 4, 5, and 6. Likewise Atlantic ocean cross section could be shown. The Pacific as the end part of the global conveyor belt circulation may give a slightly better example as it contains the oldest water and possibly a more pronounced imprint of integrated tracer sources and sinks. In Figure 7, the results for the isotope ratios  $^{231}\text{Pa}/^{230}\text{Th}$  and  $^{10}\text{Be}/^{230}\text{Th}$  in the particle loss to the sediment are given.

[14] Table 1 shows that in experiments L1 and L2 the change in  $\text{CaCO}_3$  export production is dominant, while in experiments H1 and H2 it is the opal (or BSi) production. Therefore the change in  $^{230}\text{Th}$  (Figures 4e–4h) is largest in experiments L1 and L2, while only small changes result in  $^{231}\text{Pa}$  as well as  $^{10}\text{Be}$ , and vice versa in runs H1 and H2, where changes are largest for  $^{231}\text{Pa}$  (Figures 5i–5l) and  $^{10}\text{Be}$  (Figures 6i–6l). The differences in the reaction to the composition ratio changes between the runs which allow no scavenging to POC and those who allow this, are larger the lower the particle reactivity is. While the changes in the  $^{230}\text{Th}$  distributions are quite similar for the pairs of runs L1 and L2 (see, e.g., the pair of Figures 4e and 4g), discrepancies increase between runs H1 and H2 especially for  $^{10}\text{Be}$  (compare Figures 6i and 6k). Nevertheless, in all cases with significant changes in particle species concentrations, the same trend in radionuclides is found regardless whether one uses POC as an additional carrier phase or not. The complication of scavenging to organic matter, therefore, does not preclude a use of radionuclide combinations for

potential reconstructions of particle composition ratios in the water column. Moreover, in cases with considerable concentration changes in the primary inorganic carrier phase of the specific radionuclide, the resulting changes in water column distributions are significant with respect to the absolute magnitude of the concentrations (compare, e.g., Figures 4a with 4e, 5c with 5k, and 6a with 6i). Also, the respective particle attached concentrations change significantly (Figures 4b and 4f, 5c and 5l, and 6b and 6j).

[15] The changes in the nuclide ratios  $^{231}\text{Pa}/^{230}\text{Th}$  and  $^{10}\text{Be}/^{230}\text{Th}$  of particles settling to the sediment are relatively small for the sensitivity experiments as compared with the respective standard run results (Figure 7). Apart from the polar regions, reactions in the nuclide ratios concentrate mostly on locations with substantial BSi production, i.e., upwelling areas, or regions of larger gradients in export production rain ratios. These regions are more or less limited to the equatorial Pacific Ocean (eastern and central parts) and the northwestern North Atlantic. In these limited areas, the particle composition ratio change induces a change in the sediment nuclide ratios which is significant and in the expected direction. Given that the ocean circulation would not change, this would open up a perspective for using  $^{231}\text{Pa}/^{230}\text{Th}$  and  $^{10}\text{Be}/^{230}\text{Th}$  sediment core data for estimating past particle composition ratio changes. This apparent strength, however, is turned into a weakness as soon as the ocean circulation changes. In the worst case, radionuclide changes due to variations in circulation and biological production would compensate each other: The nuclide pattern would show no change, though circulation, biological particle production, and the composition of the particle rain would in fact have changed.

[16] In our model experiments, large changes in the nuclide ratios occur especially in the Southern Ocean. The reason for this feature may be attributed to the model formulation: The choice of the switch for the  $^{230}\text{Th}$  carrier phase at low  $\text{CaCO}_3$  concentrations (see section on model description above) and the critical estimate of realistic biological export production rates in or near ice covered areas could induce an apparent overestimate of the reaction in nuclide ratios. In other words, whenever the mass fluxes in particles become small, the modeled errors in the particle composition may increase. This would not matter much as long as one would be primarily interested in simulating gross cycling of elements such as silicon and carbon, but could alienate the simulation of nuclides as well as nuclide ratios considerably. We have also carried out a run, where the threshold value for the  $^{230}\text{Th}$  particle carrier phase was not included (not shown). The results at middle or low latitudes were close to those presented here. Potential errors in the high latitude simulation therefore do not propagate largely into more equatorward regions owing to the sufficiently high particle reactivity of the nuclides involved.

[17] As an example for the timing of a reaction in radionuclides to particle composition, we show in Figure 8 a central Pacific Ocean  $^{230}\text{Th}$  time series (dissolved phase) from the model run L1 with strong reduction in the  $\text{CaCO}_3$  export. The reaction in  $^{230}\text{Th}$  activity after the perturbation is quickest in the upper ocean (450 m), but with increasing amplitude towards the deep ocean (2000 m, 4000 m). The

changes in this case indicate that even for smaller perturbations, a signal in the dissolved phase should be detectable.

## 5. Conclusion

[18] According to our model results, and if the preferential scavenging applied in the simulations is realistic, the radionuclides  $^{230}\text{Th}$ ,  $^{231}\text{Pa}$ , and  $^{10}\text{Be}$  can potentially serve as recorders of changes in the composition of particle rain. This statement seems to hold even if the radionuclides are scavenged by organic matter next to their preferential inorganic carrier substance. The regions for a successful paleoceanographic application are relatively small for sedimentary nuclide ratios and linked with upwelling systems and regions of significant horizontal gradients in rain ratios. Furthermore, the interpretation of the signal is only really useful as long as the ocean circulation would not change significantly. This “dilution” of the effect due to variations in particle composition on the nuclide concentrations limits the straightforward use of sediment nuclide data, but probably still would be useful for reconstructions of past climate evolutions through multi-tracer approaches and data assimilation methods (such as the use of adjoint models). In these cases, the nuclide ratios could add a further constraint to the inverse calculations in order to narrow down the uncertainties in the reconstructions. For the modern and future ocean, the relatively strong reaction of water column nuclide concentrations, especially as dissolved phases, to particle export composition ratio changes could perhaps become an option for monitoring potential changes in the particle export ratio which could occur as a consequence of the oceanic acidification [Royal Society, 2005; Riebesell et al., 2000; Heinze, 2004] through uptake of anthropogenic carbon from the atmosphere. We suggest to explore the possibility for selected time series measurements of nuclides within, for example, the GEOTRACES program (<http://www.ldeo.columbia.edu/res/pi/geotraces/>). Such an assessment method could be a more reliable indicator for changes in large-scale  $\text{CaCO}_3$  production than direct measurements, as the global value of  $\text{CaCO}_3$  production is not very well known even for today’s ocean.

[19] **Acknowledgments.** Two constructive anonymous reviewers helped to improve this manuscript. Support of this work through grant EVK2-CT-2001-00100 (EU FP5 RTD project “ORFOIS”) by the European Commission and through the Bjerknes Centre for Climate Research by the Norwegian Research Council is gratefully acknowledged. This is publication A 128 from the Bjerknes Centre for Climate Research. This is LSCE publication 1795.

## References

- Andersen, K. K., A. Armengaud, and C. Genthon (1998), Atmospheric dust under glacial and interglacial conditions, *Geophys. Res. Lett.*, *25*, 2281–2284.
- Antia, A. N., et al. (2001), Basin-wide particulate carbon flux in the Atlantic Ocean: Regional export patterns and potential for atmospheric  $\text{CO}_2$  sequestration, *Global Biogeochem. Cycles*, *15*(4), 845–862.
- Baumann, K.-H., H. Andruleit, B. Böckel, M. Geisen, and H. Kinkel (2005), The significance of extant coccolithophores as indicators of ocean water masses, surface water temperature, and paleoproductivity: A review, *Palaeontol. Z.*, *79*(1), 93–112.
- Berger, W. H., and R. S. Keir (1984), Glacial-Holocene changes in atmospheric  $\text{CO}_2$  and the deep-sea record, in *Climate Processes and Climate Sensitivity*, *Geophys. Monogr.*, vol. 29, edited by J. E. Hansen and T. Takahashi, pp. 337–351, AGU, Washington, D. C.
- Brost, R. A., J. Feichter, and M. Heimann (1991), Three-dimensional simulation of  $^{10}\text{Be}$  in a global climate model, *J. Geophys. Res.*, *96*, 22,423–22,445.
- Chase, Z., R. F. Anderson, M. Q. Fleisher, and P. W. Kubik (2002), The influence of particle composition and particle flux on scavenging of Th, Pa and Be in the ocean, *Earth Planet. Sci. Lett.*, *204*, 215–229.
- Chase, Z., R. F. Anderson, M. Q. Fleisher, and P. W. Kubik (2003), Scavenging of  $^{230}\text{Th}$ ,  $^{231}\text{Pa}$ , and  $^{10}\text{Be}$  in the Southern Ocean (SW Pacific sector): The importance of particle flux, particle composition and advection, *Deep Sea Res., Part II*, *50*, 739–768.
- Dymond, J., and M. Lyle (1985), Flux comparisons between sediments and sediment traps in the eastern tropical Pacific: Implications for atmospheric  $\text{CO}_2$  variations during the Pleistocene, *Limnol. Oceanogr.*, *30*, 699–712.
- Feichter, J., R. Brost, and M. Heimann (1991), Three-dimensional modeling of the concentration and deposition of  $^{210}\text{Pb}$ , *J. Geophys. Res.*, *96*, 22,447–22,460.
- Frank, M., M. M. Rutgers van der Loeff, P. W. Kubik, and A. Mangini (2002), Quasi-conservative behaviour of  $^{10}\text{Be}$  in deep waters of the Weddell Sea and the Atlantic sector of the Antarctic Circumpolar Current, *Earth Planet. Sci. Lett.*, *201*, 171–186.
- Gehlen, M., C. Heinze, E. Maier-Reimer, and C. I. Measures (2003), Coupled Al-Si geochemistry in an ocean general circulation model: A tool for the validation of oceanic dust deposition?, *Global Biogeochem. Cycles*, *17*(1), 1028, doi:10.1029/2001GB001549.
- Hanson, R. B., H. W. Ducklow, and J. G. Field (Eds.) (2000), *The Changing Ocean Carbon Cycle—A Midterm Synthesis of the Joint Global Ocean Flux Study*, *Int. Geosphere-Biosphere Programme Book Ser.*, vol. 5, 514 pp., Cambridge Univ. Press, New York.
- Heinze, C. (2004), Simulating oceanic  $\text{CaCO}_3$  export production in the greenhouse, *Geophys. Res. Lett.*, *31*, L16308, doi:10.1029/2004GL020613.
- Heinze, C., and E. Maier-Reimer (1999), The Hamburg Oceanic Carbon Cycle Circulation Model Version “HAMOCC2s” for long time integrations, *Tech. Rep. 20*, 7 pp., German Clim. Comput. Cent., Hamburg, Germany.
- Heinze, C., E. Maier-Reimer, A. M. E. Winguth, and D. Archer (1999), A global oceanic sediment model for long-term climate studies, *Global Biogeochem. Cycles*, *13*(1), 221–250.
- Heinze, C., A. Hupe, E. Maier-Reimer, N. Dittert, and O. Ragueneau (2003), Sensitivity of the marine biospheric Si cycle for biogeochemical parameter variations, *Global Biogeochem. Cycles*, *17*(3), 1086, doi:10.1029/2002GB001943.
- Henderson, G. M., C. Heinze, R. F. Anderson, and A. M. E. Winguth (1999), Global distribution of the  $^{230}\text{Th}$  flux to ocean sediments constrained by GCM modelling, *Deep Sea Res., Part I*, *46*, 1861–1893.
- Honeyman, B. D., L. S. Balistrieri, and J. W. Murray (1988), Oceanic trace metal scavenging: The importance of particle concentration, *Deep Sea Res.*, *35*, 227–246.
- Koch, D. M., D. J. Jacob, and W. C. Graustein (1996), Vertical transport of tropospheric aerosols as indicated by  $^{7}\text{Be}$  and  $^{210}\text{Pb}$  in a chemical tracer model, *J. Geophys. Res.*, *101*, 18,651–18,666.
- Ku, T. L., M. Kusakabe, C. I. Measures, J. R. Southon, G. Cusimano, J. S. Vogel, D. E. Nelson, and S. Nakaya (1990), Beryllium isotope distribution in the western North Atlantic: A comparison to the Pacific, *Deep Sea Res.*, *37*, 795–808.
- Kusakabe, M., T. L. Ku, J. R. Southon, J. S. Vogel, D. E. Nelson, C. I. Measures, and Y. Nozaki (1987), Distribution of  $^{10}\text{Be}$  and  $^{9}\text{Be}$  in the Pacific Ocean, *Earth Planet. Sci. Lett.*, *82*, 231–240.
- Lal, D., and B. Peters (1967), Cosmic ray produced radioactivity on the Earth, in *Handbuch der Physik*, vol. XLVI/2, pp. 551–612, Springer, New York.
- Land, C., and J. Feichter (2003), Stratosphere-troposphere exchange in a changing climate simulated with the general circulation model MAECHAM4, *J. Geophys. Res.*, *108*(D12), 8523, doi:10.1029/2002JD002543.
- Li, Y.-H. (2005), Controversy over the relationship between major components of sediment-trap materials and the bulk distribution coefficient of  $^{230}\text{Th}$ ,  $^{231}\text{Pa}$ , and  $^{10}\text{Be}$ , *Earth Planet. Sci. Lett.*, *233*, 1–7.
- Luo, S., and T.-L. Ku (1999), Oceanic  $^{231}\text{Pa}/^{230}\text{Th}$  ratio influenced by particle composition and remineralisation, *Earth Planet. Sci. Lett.*, *167*, 183–195.
- Maier-Reimer, E. (1993), Geochemical cycles in an ocean general circulation model: Preindustrial tracer distributions, *Global Biogeochem. Cycles*, *7*, 645–677.
- Maier-Reimer, E., U. Mikolajewicz, and K. Hasselmann (1993), Mean circulation of the Hamburg LSG OGCM and its sensitivity to the thermal surface forcing, *J. Phys. Oceanogr.*, *23*, 731–757.

- Masarik, J., and J. Beer (1999), Simulation of particle fluxes and cosmogenic nuclide production in the Earth's atmosphere, *J. Geophys. Res.*, *104*, 12,099–12,111.
- Oeschger, H., J. Houtermann, H. Loosli, and M. Wahlen (1969), The constancy of cosmic radiation from isotope studies in meteorites and on the Earth, in *Radiocarbon Variations and Absolute Chronology*, edited by I. Olsen, John Wiley, Hoboken, N. J.
- Quigley, M. S., P. H. Santschi, C.-C. Hung, L. Gua, and B. D. Honeyman (2002), Importance of polysaccharides for  $^{234}\text{Th}$  complexation to organic matter, *Limnol. Oceanogr.*, *47*, 367–377.
- Riebesell, U., I. Zondervan, B. Rost, P. D. Tortell, R. E. Zeebe, and F. M. M. Morel (2000), Reduced calcification of marine plankton in response to increased atmospheric  $\text{CO}_2$ , *Nature*, *407*, 364–367.
- Royal Society (2005), Ocean acidification due to increasing atmospheric carbon dioxide, *Policy Doc. 12/05*, 60 pp., London.
- Scholten, J. C., J. Fietzke, S. Vogler, M. M. Rutgers van der Loeff, A. Mangini, W. Koeve, J. Waniek, P. Stoffers, A. Antia, and J. Kuss (2001), Trapping efficiencies of sediment traps from the deep Eastern North Atlantic: The  $^{230}\text{Th}$  calibration, *Deep Sea Res., Part II*, *48*, 2383–2408.
- Scholten, J. C., et al. (2005), Radionuclide fluxes in the Arabian Sea: The role of particle composition, *Earth Planet. Sci. Lett.*, *48*, 2383–2408.
- Winguth, A. M. E., D. Archer, J.-C. Duplessy, E. Maier-Reimer, and U. Mikolajewicz (1999), Sensitivity of paleonutrient tracer distributions and deep sea circulation to glacial boundary conditions, *Paleoceanography*, *14*, 304–323.
- 
- M. Gehlen, Laboratoire des Sciences du Climat et de L'Environnement, UMR CEA-CNRS, CE Saclay/Orme des Merisiers Bat.709, F-91191 Gif-sur-Yvette, France. (gehlen@lsce.saclay.cea.fr)
- C. Heinze, Geophysical Institute and Bjerknes Centre for Climate Research, University of Bergen, Allégaten 70, N-5007 Bergen, Norway. (heinze@gf.uib.no)
- C. Land, Meteoterra GmbH, Im Poll 8, D-31737 Rinteln/Exten, Germany. (ch.land@meteoterra.de)